

# Chandrasekhar Theory of Ellipsoidal Electromagnetic Scatterers

Peter B. Weichman

*BAE Systems, Advanced Information Technologies,  
6 New England Executive Park, Burlington, MA 01803*

A number of new problems in remote sensing and identification of buried compact metallic targets motivate the search for new models that, if not exact, at least enable extremely rapid numerical predictions of electromagnetic scattering/induction data. Here the elegant Chandrasekhar theory of the electrostatics of charged ellipsoids is used to develop an essentially exact, extremely efficient description of low- to intermediate frequency (or late- to intermediate-time) responses of ellipsoidal targets. Comparisons with experimental data demonstrate that, together with a previously developed theory of the high frequency (or early time) regime, the results serve to cover the entire dynamic range encountered in typical measurements.

Exactly soluble models in the theory of EM propagation and scattering are essentially limited to horizontally stratified or spherically symmetric geometries, with limited results also available for cylindrically symmetric waveguide geometries [1]. However, there are a number of new problems in remote sensing and classification of buried compact metallic targets that require a wider class of solutions that, if not exact, at least support rapid numerical evaluation. These include a number of long-standing economic and humanitarian problems, such as clearance of unexploded ordnance (UXO) from old test ranges. The most difficult technological issue is *not* the detection of such targets, but rather the ability to distinguish between them and harmless clutter items, such as pieces of exploded ordnance. Since clutter tends to exist at much higher density, even modest discrimination ability leads to huge reductions in remediation costs.

The most promising technologies, least influenced by the complexities of the heterogeneous earth, are essentially low frequency ( $< 10$  kHz) metal detectors that emit a series of sharply terminated, well spaced pulses, and measure the decaying induced currents during the ( $\sim 25$  ms) quiet interval between pulses. At these low frequencies, detailed spatial resolution is lost [2], but the induced voltage curve  $V(t)$  has substantial structure, and one may hope to extract target geometry information from it. This inference, however, is indirect [3] and solution of this inverse problem requires careful comparison of predicted and measured responses. This requires accurate models that go well beyond existing exact solutions.

A number of classes of buried objects, especially UXO, have a cylindrical geometry. As a step in the direction of modeling such objects, I consider here EM scattering from ellipsoids, with arbitrary axes  $\mathbf{a} = (a_1, a_2, a_3)$ . Although fully analytic solutions are not possible [4], it is demonstrated here that Chandrasekhar's elegant approach to the electrostatics of heterogeneously charged ellipsoids [5] enables the major part of the computation to be performed analytically, reducing it to a matrix diagonalization problem. The size of the matrix grows as one pushes earlier in time, closer to pulse termination (where the high frequency components of the pulse spec-

trum have not yet had a chance to decay away), but enables an essentially exact description at intermediate- to late-time at minimal numerical cost. As will be demonstrated through comparisons with laboratory data on artificial spheroidal targets, combining this approach with a complementary early-time approach [6] enables accurate predictions at all time (or frequency) scales.

For clarity of exposition, the theory will be presented for nonmagnetic target and background,  $\mu = \mu_b$ , where  $\mu_b$  is the (uniform) background permeability. Magnetic targets exhibit both a conductivity and a permeability contrast, which complicates the analysis but does not affect the basic approach. Details of this generalization will be presented elsewhere.

For nonmagnetic systems, the Maxwell equations may be reduced, in the frequency domain, to a single equation for the electric field

$$\nabla \times \nabla \times \mathbf{E} - \kappa^2 \mathbf{E} = \mathbf{S}, \quad (1)$$

where  $\kappa^2 = \epsilon \mu k^2$ ,  $k = \omega/c$ , and source term  $\mathbf{S} = (4\pi i \mu k/c) \mathbf{j}_S$  where  $\mathbf{j}_S$  is the source current density, representing in this case the transmitter coil. Inside the metallic target, at all frequencies of interest here, the dielectric function is dominated by the dc conductivity,  $\epsilon = 4\pi i \sigma/\omega$ . The background may be insulating or weakly conducting, but we work in the very high contrast limit  $|\epsilon/\epsilon_b| \gg 1$  [7].

To obtain a closed equation, restricted to the finite target domain  $V_c$ , we use the Green function approach. A background field  $\mathbf{E}_b$  is defined by solving (1) for the same source  $\mathbf{S}$ , but in the absence of a target,  $\kappa^2 = \kappa_b^2$ . By subtracting this equation from (1), and applying the background tensor Green function  $\hat{\mathbf{G}}$ , defined by

$$\nabla \times \nabla \times \hat{\mathbf{G}}(\mathbf{x}, \mathbf{x}') - \kappa_b^2 \hat{\mathbf{G}}(\mathbf{x}, \mathbf{x}') = \mathbb{1} \delta(\mathbf{x} - \mathbf{x}'), \quad (2)$$

where  $\mathbb{1}$  is the  $3 \times 3$  identity matrix and the curls act on the first index of  $\hat{\mathbf{G}}$ , (1) takes the integral form

$$\mathbf{E}(\mathbf{x}) = \mathbf{E}_b(\mathbf{x}) + \int_{V_c} d^3 x' Q(\mathbf{x}') \hat{\mathbf{G}}(\mathbf{x}, \mathbf{x}') \cdot \mathbf{E}(\mathbf{x}'), \quad (3)$$

where the contrast function  $Q = \kappa^2 - \kappa_b^2$  vanishes outside the target volume  $V_c$ . For a uniform background

one obtains  $\hat{\mathbf{G}} = (\mathbb{1} + \kappa_b^{-2} \nabla \nabla) g$ , where  $g(\mathbf{x}, \mathbf{x}') = e^{i\kappa_b |\mathbf{x} - \mathbf{x}'|} / 4\pi |\mathbf{x} - \mathbf{x}'|$  is the scalar Helmholtz Green function. Restricting  $\mathbf{x} \in V_c$ , (3) becomes an equation for the internal field  $\mathbf{E}_{\text{int}}$  alone. Given  $\mathbf{E}_{\text{int}}(\mathbf{x})$ , the external field  $\mathbf{E}_{\text{ext}}(\mathbf{x})$ ,  $\mathbf{x} \notin V_c$ , follows by direct integration.

Over the measurement domain outside  $V_c$ ,  $\kappa_b$  can vary strongly, encompassing soil, rock, surface plants, air, etc. The full  $\mathbf{E}$  field is therefore unpredictable. However, an EM induction (EMI) measurement is sensitive only to the ‘‘magnetic’’ contribution to  $\mathbf{E}$ . Specifically, one may divide  $\mathbf{E}$  into curl-free and divergence free contributions, and in the high contrast limit equation (3) reduces to [8]

$$\mathbf{E}(\mathbf{x}) - \mathbf{E}_b(\mathbf{x}) = \int_{V_c} d^3 x' \frac{\kappa(\mathbf{x}')^2 \mathbf{E}(\mathbf{x}')}{4\pi |\mathbf{x} - \mathbf{x}'|} - \nabla \varphi(\mathbf{x}), \quad (4)$$

in which the potential term  $\nabla \varphi$ , which depends on the detailed form of  $\kappa_b$ , is explicitly curl free, and it follows from (1) that the divergence of the first term is of relative order  $\kappa_b^2 / \kappa^2$  [9]. It follows as well that (4) enforces the boundary condition  $\mathbf{E}_{\text{int}} \cdot \hat{\mathbf{n}} = O(\epsilon_b / \epsilon) \rightarrow 0$ , where  $\hat{\mathbf{n}}$  is the unit surface normal. The background  $\mathbf{E}_b$  is to be treated as a known input here.

Remarkably, there is a straightforward procedure for solving (4) that entirely avoids computing  $\varphi$ , or the non-inductive part of  $\mathbf{E}_b$ . Thus, let  $\{\mathbf{Z}_N(\mathbf{x})\}_{N=1}^\infty$  be a complete set of basis functions supported on  $V_c$ , and obeying  $\nabla \cdot \mathbf{Z}_N = 0$ ,  $\mathbf{x} \in V_c$ , and  $\hat{\mathbf{n}} \cdot \mathbf{Z}_N = 0$ ,  $\mathbf{x} \in \partial V_c$ . One may then expand

$$\kappa(\mathbf{x})^2 \mathbf{E}_{\text{int}}(\mathbf{x}) = \sum_N \zeta_N \mathbf{Z}_N(\mathbf{x}). \quad (5)$$

The key observation is that the inner product  $\int_{V_c} d^3 x \mathbf{Z}_n \cdot \nabla f \equiv 0$  for any scalar function  $f$ . Therefore, inserting (5) into (4) and taking the inner product on the left with  $\mathbf{Z}_M^*$ , one obtains the matrix equation

$$(i\omega \hat{\mathcal{O}} - \hat{\mathcal{L}}) \boldsymbol{\zeta} = \boldsymbol{\zeta}_b, \quad (6)$$

where the self-adjoint arrays  $\hat{\mathcal{O}}$ ,  $\hat{\mathcal{L}}$  are defined by

$$\begin{aligned} \hat{\mathcal{O}}_{MN} &= - \int_{V_c} d^3 x \frac{\mathbf{Z}_M(\mathbf{x})^* \cdot \mathbf{Z}_N(\mathbf{x})}{4\pi \mu \sigma(\mathbf{x})} \\ \hat{\mathcal{L}}_{MN} &= \int_{V_c} d^3 x \int_{V_c} d^3 x' \frac{\mathbf{Z}_M(\mathbf{x})^* \cdot \mathbf{Z}_N(\mathbf{x}')}{4\pi |\mathbf{x} - \mathbf{x}'|} \\ \zeta_{b,M} &= \int_{V_c} d^3 x \mathbf{Z}_M(\mathbf{x})^* \cdot \mathbf{E}_b(\mathbf{x}). \end{aligned} \quad (7)$$

Given the solution of this equation for the amplitude array  $\boldsymbol{\zeta}$ , the result of an external magnetic field or EMI measurement is also independent of  $\varphi$ . The curl in the magnetic field relation  $\mathbf{B} = (i\omega)^{-1} \nabla \times \mathbf{E}$  annihilates  $\nabla \varphi$ , while an induced voltage measurement involves a line integral around the closed receiver loop  $C_R$ , which is also insensitive to any gradient contribution.

Now, in the time domain, one is primarily interested in freely decaying signals when  $\mathbf{S}, \mathbf{E}_b$ , hence  $\boldsymbol{\zeta}_b$ , vanish.

One seeks solutions in the form of a mode expansion  $\mathbf{E} = \sum_n A_n \mathbf{E}^{(n)}(\mathbf{x}) e^{-\lambda_n t}$ , in which each (normalized) mode shape  $\mathbf{E}^{(n)}$  is expanded in the form (5), and the decay rates  $\lambda_n$  and corresponding basis function coefficients  $\boldsymbol{\zeta}^{(n)}$  are solutions to the generalized eigenvalue equation,

$$\hat{\mathcal{L}} \boldsymbol{\zeta} = \lambda \hat{\mathcal{O}} \boldsymbol{\zeta}. \quad (8)$$

Using mode orthogonality it can be shown that the excitation coefficients  $A_n$  are given by

$$A_n = I_T^{(n)} \oint_{C_T} \mathbf{E}^{(n)*} \cdot d\mathbf{l}, \quad I_T^{(n)} \equiv - \int_{-\infty}^0 dt e^{\lambda_n t} \partial_t I_T(t), \quad (9)$$

in which  $C_T$  is the closed transmitter loop, and  $I_T(t)$  is the transmitter pulse, terminated at  $t = 0$ . The measured EMI voltage is also a multiexponential sum, with amplitudes given by similar line over  $C_R$ :

$$V_R(t) = \sum_n V_n e^{-\lambda_n t}, \quad V_n = A_n \oint_{C_R} \mathbf{E}^{(n)} \cdot d\mathbf{l}. \quad (10)$$

For general targets, explicit forms for the  $\mathbf{Z}_N$  may be hard to come by, and for general  $\sigma(\mathbf{x})$ , the integrals in (7) must be done numerically. However, for uniform, ellipsoidal targets both of these problems are absent. First, let  $\mathbf{Z}_N^{(\text{sph})}$  be basis functions for the unit sphere. We will use the forms  $\mathbf{Z}_{lmp}^{(i)}$ ,  $i = 1, 2$ , defined by [10]

$$\begin{aligned} \mathbf{Z}_{lmp}^{(1)}(\mathbf{x}) &= r^{l+2p} \mathbf{X}_{lm}(\theta, \phi) \\ \mathbf{Z}_{lmp}^{(2)}(\mathbf{x}) &= \nabla \times [(1 - r^2) r^{l+2p} \mathbf{X}_{lm}(\theta, \phi)] \end{aligned} \quad (11)$$

where  $\mathbf{X}_{lm}$  are the vector spherical harmonics [1], and  $p = 0, 1, 2, \dots$ . For an ellipsoid the forms

$$\mathbf{Z}_N(\mathbf{x}) = \sum_{\alpha=1}^3 a_\alpha \mathbf{Z}_{N,\alpha}^{(\text{sph})}(x_1/a_1, x_2/a_2, x_3/a_3) \hat{\mathbf{e}}_\alpha \quad (12)$$

have the desired properties, where  $\hat{\mathbf{e}}_\alpha$  are unit vectors along the principal directions.

The key property is that  $\mathbf{Z}_N^{(\text{sph})}$  are *polynomials* (of degree  $l + 2p$ ), and hence so are  $\mathbf{Z}_N$ , and, as advertised, the Chandrasekhar approach [5] allows Coulomb integrals of the form in (4) to be performed analytically. The inner product of this result with another basis function, as in (7), is then trivial to compute. The method is elegant, but somewhat intricate, and so will only be outlined here. The basic result we use is [5]:

$$\begin{aligned} \phi(\mathbf{x}) &\equiv \int d^3 x' \frac{\rho[\mu(\mathbf{x}')] }{|\mathbf{x} - \mathbf{x}'|} \\ &= \int_{\tau(\mathbf{x})}^{\infty} dt \frac{\psi(1) - \psi[\mu(t; \mathbf{x})]}{\sqrt{(a_1^2 + t)(a_2^2 + t)(a_3^2 + t)}}, \end{aligned} \quad (13)$$

where  $\rho$  is any 1D function of the quantity  $\mu(\mathbf{x}) = \sum_\alpha x_\alpha^2 / a_\alpha^2 \in [0, 1]$ , which traces out the family of similar ellipsoids inside  $V_c$ ,  $\psi(\mu) = \int_0^\mu \rho(\mu') d\mu'$  is the antiderivative of  $\rho$ ,  $\mu(t, \mathbf{x}) = \sum_\alpha x_\alpha^2 / (a_\alpha^2 + t) \in [0, 1]$ , and

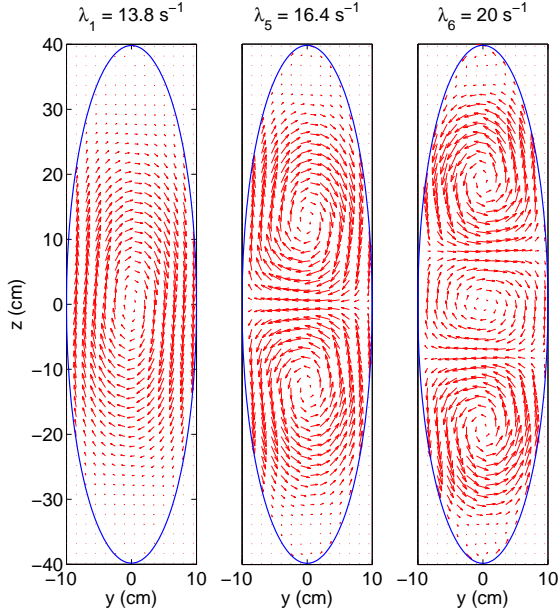


FIG. 1: (Color online) Three lowest order vertically circulating mode shapes, and corresponding decay rates, for a  $10 \times 10 \times 40$  cm radius aluminum prolate spheroid:  $(E_y, E_z)$  are plotted in the  $x = 0$  plane.

$\tau(\mathbf{x}) \equiv 0$  for  $\mathbf{x} \in V_c$ , and is otherwise the solution to  $1 = \sum_{\alpha=1}^3 x_{\alpha}^2 / (a_{\alpha}^2 + \tau)$ ,  $\mathbf{x} \notin V_c$ , which defines the family of confocal ellipsoids surrounding  $V_c$ .

We apply this relation to compute potentials  $\phi_n$  due to monomial densities of the form  $\rho_n(\mu) = (1 - \mu)^n / n!$ , so that  $\psi_n(1) - \psi_n(\mu) = \rho_{n+1}(\mu)$ . The density in (13) is then a polynomial of degree  $2n$ . To isolate a single monomial, one takes a combination of derivatives with respect to  $\mathbf{x}$  and  $a_{\alpha}^{-2}$ :

$$\begin{aligned} D_{2\mathbf{l}+\mathbf{m}}(\mathbf{x}) &\equiv \int_{V_c} d^3x' \frac{\prod_{\alpha} x_{\alpha}^{2l_{\alpha}+m_{\alpha}}}{|\mathbf{x} - \mathbf{x}'|} \\ &= (-1)^{|\mathbf{l}+\mathbf{m}|} \partial_{\mathbf{a}}^{\mathbf{l}} \left[ \prod_{\alpha} \left( \frac{a_{\alpha}^2}{2} \partial_{\alpha} \right)^{m_{\alpha}} \right] \phi_{|\mathbf{l}+\mathbf{m}|}(\mathbf{x}) \\ &= \sum'_{\mathbf{k}} D_{2\mathbf{k}+\mathbf{m}}^{(2\mathbf{l}+\mathbf{m})}(\tau) \prod_{\alpha} x_{\alpha}^{2k_{\alpha}+m_{\alpha}}, \end{aligned} \quad (14)$$

where  $\mathbf{l} = (l_1, l_2, l_3)$  is a vector of nonnegative integers,  $\mathbf{m} = (m_1, m_2, m_3)$  with each  $m_{\alpha} = 0$  or  $1$ ,  $|\mathbf{l} + \mathbf{m}| = \sum_{\alpha} (l_{\alpha} + m_{\alpha})$ ,  $\partial_{\mathbf{a}}^{\mathbf{l}} = \prod_{\alpha} (-1)^{l_{\alpha}} \partial^{l_{\alpha}} / \partial (a_{\alpha}^{-2})^{l_{\alpha}}$ , the primed sum is restricted to  $|\mathbf{k}| \leq |\mathbf{l}| + 1$ , and

$$\begin{aligned} D_{2\mathbf{k}+\mathbf{m}}^{(2\mathbf{l}+\mathbf{m})}(\tau) &= \frac{\pi a_1 a_2 a_3}{(|\mathbf{l}| - |\mathbf{k}| + 1)!} \sum'_{\mathbf{p}} A_{\mathbf{k}+\mathbf{m}+\mathbf{p}}(\tau) \\ &\quad \times \prod_{\alpha} C_{p_{\alpha}}^{(k_{\alpha} l_{\alpha} m_{\alpha})} a_{\alpha}^{2(l_{\alpha}+m_{\alpha}+p_{\alpha})}, \end{aligned} \quad (15)$$

where the primed sum is over all  $0 \leq p_{\alpha} \leq l_{\alpha}$ , and the

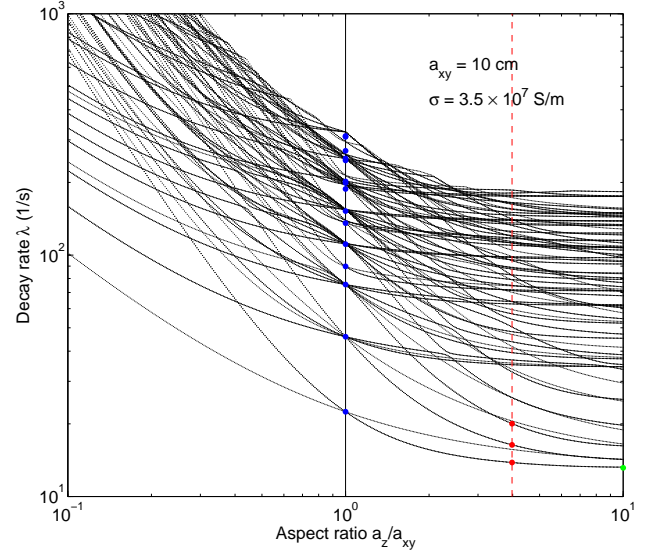


FIG. 2: (Color online) Decay rate spectrum vs. aspect ratio  $\alpha = a_z/a_{xy}$ , with fixed conductivity and radius  $a_{xy}$ . The first 125 decay rates (computed using 232 basis functions) are plotted for each  $0.1 \leq \alpha \leq 10$ . Blue dots at  $\alpha = 1$  show exact analytic results for the sphere, with degeneracy effects from enhanced symmetry evident. Red dots at  $\alpha = 4$  mark the three modes shown in Fig. 1 (three other nearby modes circulate around the cylinder axis, rather than along it). Green dot at the right is the analytic result for the lowest mode for an infinite cylinder,  $\alpha \rightarrow \infty$ . More slowly increasing branches at the left,  $\alpha \ll 1$ , correspond to modes with current patterns circulating in the  $xy$ -plane.

combinatorial factor is

$$C_p^{(klm)} = \frac{(-1)^{k+l}}{k!} \binom{l}{p} \frac{\Gamma(\frac{1}{2} - m - p) \Gamma(k + m + p + \frac{1}{2})}{\Gamma(\frac{1}{2} - m - l) \Gamma(k + m + \frac{1}{2})}. \quad (16)$$

Finally, the elliptic-type integrals are defined by

$$A_{\mathbf{k}}(\tau) = \int_{\tau}^{\infty} \frac{dt}{\prod_{\alpha} (a_{\alpha}^2 + t)^{k_{\alpha} + \frac{1}{2}}}. \quad (17)$$

These obey the iterative relation  $\partial A_{\mathbf{k}} / \partial a_{\alpha}^2 = -(k_{\alpha} + \frac{1}{2}) A_{\mathbf{k} + \hat{\mathbf{e}}_{\alpha}}$ , and evaluation may be reduced to that of  $A(\mathbf{a}, \tau) \equiv A_{\mathbf{0}}$ . With the convention  $a_1 \geq a_2 \geq a_3$  one obtains  $A(\mathbf{a}, \tau) = 2F(\theta, q) / \sqrt{a_1^2 - a_3^2}$ , in which  $F$  is the elliptic integral [11],  $\sin^2(\theta) = \sqrt{(a_1^2 - a_3^2) / (a_1^2 + \tau)}$  and  $q^2 = (a_1^2 - a_2^2) / (a_1^2 - a_3^2)$ . Derivatives of  $F$ , and the auxiliary elliptic integral  $E(\varphi, k)$  [11], may be expressed back in terms of  $E, F$ , allowing (17) to be evaluated by iteration. In the case of spheroids,  $a_1 = a_2$  or  $a_2 = a_3$ , fully analytic expressions for  $E, F$  are available [11].

Numerical implementation proceeds as follows: (a) Use the polynomial forms (11), (12) and Coulomb integrals (14), (15) (with  $\tau = 0$ ) to assemble (truncated) arrays  $\hat{\mathcal{O}}, \hat{\mathcal{L}}$ . (b) Solve the eigenvalue equation (8) for the decay rates and (internal) mode shapes. (c) Use the known transmitter geometry and pulse waveform to compute the

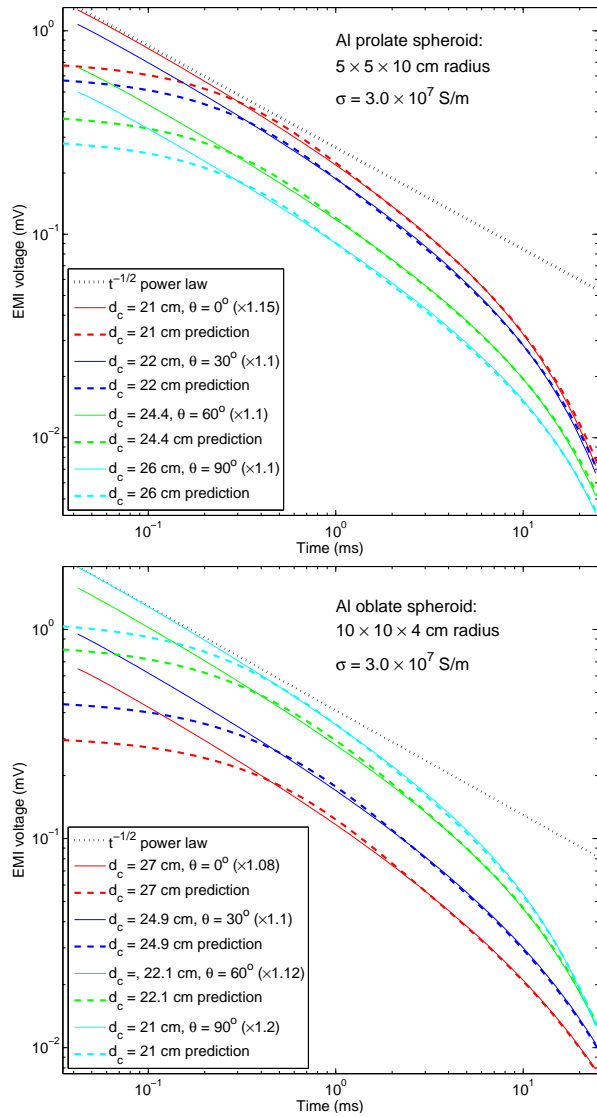


FIG. 3: (Color online) Comparisons of data (solid lines; taken by the NRL TEMTADS platform [12]) and theoretical predictions (dashed lines) for a  $5 \times 5 \times 10$  cm radius aluminum prolate spheroid (top) and a  $10 \times 10 \times 4$  cm radius aluminum oblate spheroid (bottom), at various depths-to-center  $d_c$ , with various axial tilt angles  $\theta$ . The multipliers indicated in each legend entry reflect a  $\sim 10\%$  variability in the transmitter current, and are applied to the data to optimize the fit. Straight dashed lines show the predicted  $1/\sqrt{t}$  early time divergence [6]. This first principles agreement, over nearly two decades in both time and voltage, is remarkable.

excitation coefficients (9). This involves an external field computation, the Coulomb integral of  $\mathbf{E}_{\text{int}}$  in (4), which follows from (14), (15) with  $\tau > 0$ . (d) Finally, use the known receiver geometry to compute the voltage (10).

Figure 1 shows three of the computed mode shapes, obtained using the 232 basis functions (11) corresponding to  $1 \leq l+2p \leq 7$ . Figure 2 shows the computed decay rate spectrum for a two decade range of spheroid aspect ratios. Figure 3 describes comparisons with experimental

data from aluminum spheroids. The truncation loses accuracy at early time since more rapidly decaying modes with more complex geometry are not properly captured. However, the predictions merge smoothly with those of the complementary early time theory [6], which predicts a  $1/\sqrt{t}$  divergence. The combined result yields an excellent fit over the full dynamic range. With this level of agreement (afforded equally by the present theory and the remarkable hardware improvement [12]), the subtle changes in curve shape with depth and orientation can indeed be inverted for target geometry. This will be discussed in detail elsewhere.

The author thanks Daniel Steinhurst for providing experimental data. This work was supported by SERDP, through the US Army Corps of Engineers, Humphreys Engineer Center Support Activity under Contract No. W912HQ-09-C-0024.

- 
- [1] See, e.g., J. D. Jackson *Classical Electrodynamics* (John Wiley and sons, New York, 1975).
  - [2] Ground penetrating radar operating at GHz frequencies provides some imaging capability, but works well only over dry, homogeneous ground (e.g., sand or concrete).
  - [3] Metallic EM skin depths at  $O(10 \text{ Hz})$  are  $O(10 \text{ cm})$ . The response on  $O(10 \text{ ms})$  time scales then indirectly reflects target geometry on this scale. An analogy is the famous problem of “hearing the shape of a drum,” i.e., determining its boundary from its vibration spectrum.
  - [4] Ellipsoidal coordinates enable exact solutions of certain scalar field problems, but the equations fail to separate for vector fields. See, e.g., P. M. Morse and H. Feshbach, *Methods of Theoretical Physics* (McGraw Hill, 1953).
  - [5] S. Chandrasekhar, *Ellipsoidal figures of equilibrium* (Dover, 1958).
  - [6] At very early time, the induced screening currents are confined to the target surface, and a theory may be developed based on their subsequent inward diffusion: P. B. Weichman, Phys. Rev. Lett. **91**, 143908 (2003); P. B. Weichman, Phys. Rev. Lett. **93**, 023902 (2004).
  - [7] Typical metallic and ground conductivities are  $\sigma \sim 10^7 \text{ S/m}$ ,  $\sigma_b \sim 0.1 \text{ S/m}$ , hence  $|\epsilon/\epsilon_b| = O(10^8)$ .
  - [8] Equation (4) treats  $\mathbf{E}_{\text{ext}}$  as quasistatic, neglecting wave propagation effects. Magnetic fields due to target currents, e.g., then obey the Biot-Savart law. This is valid so long as the measurement region is smaller than the background EM penetration depth, typically  $O(10\text{-}100 \text{ m})$ .
  - [9] An equation for  $\varphi$  is obtained by multiplying (4) by  $\kappa_b^2$  and taking the divergence. However, this equation, producing finite  $\varphi$  even in the limit  $\kappa_b/\kappa \rightarrow 0$ , plays no role in what follows, and so will not be discussed further.
  - [10] One may construct  $\mathbf{Z}_M$  from ellipsoidal harmonics, but these fail to diagonalize the system (6) or (8) [4]. Their desirable properties are more than compensated by the analytic simplicity of the spherical harmonics.
  - [11] I. S. Gradshteyn and I. M. Ryzhik, *Table of Integrals, Series, and Products* (Academic Press, New York, 1981).
  - [12] See, e.g., “EMI Array for Cued UXO Discrimination” at <http://serdp-estcp.org/>.